Relaxation timescales and decay of correlations in a long-range interacting quantum simulator

Mauritz van den Worm,[1] Brian C. Sawyer,[2] John J. Bollinger,[2] and Michael Kastner[1,3,*]

[1] *Institute of Theoretical Physics, University of Stellenbosch, Stellenbosch 7600, South Africa*
[2] *US National Institute of Standards and Technology, Boulder, Colorado 80305, USA*
[3] *National Institute for Theoretical Physics (NITheP), Stellenbosch 7600, South Africa*

(Dated: November 21, 2012)

We study the time evolution of correlation functions in long-range interacting quantum Ising models. For a class of initial conditions, exact analytic results are obtained in arbitrary lattice dimension, both for ferromagnetic and antiferromagnetic coupling, and hence also in the presence of geometric frustration. In contrast to the nearest-neighbor case, we find that correlations decay in time like stretched or compressed exponentials. Provided the long-range character of the interactions is sufficiently strong, pronounced prethermalization plateaus are observed and relaxation time scales are widely separated. Specializing to a triangular lattice in two spatial dimensions, we propose to utilize these results for benchmarking of a recently developed ion-trap based quantum simulator.

PACS numbers: 03.67.Ac, 05.70.Ln, 75.10.Jm, 37.10.Ty

When a physical system is coupled to a heat bath, one expects to observe thermalization to an equilibrium state whose temperature is determined by the bath properties. For an isolated many-body system, i.e., in the absence of a heat bath, the situation is less clear, although some kind of relaxation to equilibrium may be expected for sufficiently large generic systems and suitable observables. Recent progress in experiments with cold atoms and ions [1] has stimulated intense theoretical interest in equilibration and thermalization behavior of isolated many-body quantum systems [2, 3]. General mechanisms leading to thermalization have been proposed [4], rigorous proofs of equilibration have been obtained for generic Hamiltonians [5], and analytic as well as numeric model studies have been reported (see [3] for a list of references). Much less is known about the time scales on which relaxation to equilibrium takes place. In this Letter we study the time evolution of correlation functions in isolated long-range interacting quantum Ising systems on arbitrary lattices. We derive exact analytic results that further our understanding of different relaxation timescales and general nonequilibrium properties of long-range interacting systems.

Apart from broadening the theoretical understanding, our results may also prove beneficial for the interpretation of data from cold atom or ion experiments. Specializing to a triangular lattice in two spatial dimensions, we propose to utilize our results for benchmarking a recently developed ion-trap based quantum simulator [6]. This quantum simulator consists of several hundred beryllium ions stored in a Penning trap and confined to a planar slab. Due to their mutual electrostatic repulsion, the ions arrange into a two-dimensional Coulomb crystal on a triangular lattice (see Fig. 1). The valence electron spins of the $^9Be^+$ ions are the relevant degrees of freedom used for quantum simulation. Effective interactions between these spins are induced by transverse motional modes of the Coulomb crystal. Under the assumption of small, coherent ion displacements, it was shown in Refs. [7, 8] that the resulting interactions are described by the Ising Hamiltonian

$$H = -\sum_{i<j} J_{i,j}\sigma_i^z\sigma_j^z - \boldsymbol{B}_\mu \cdot \sum_i \boldsymbol{\sigma}_i. \tag{1}$$

Here i and j label the N ions on the triangular lattice, $\boldsymbol{\sigma}_i = (\sigma_i^x, \sigma_i^y, \sigma_i^z)$ denotes the vector of Pauli matrices for ion i, the $J_{i,j}$ are coupling coefficients, and $\boldsymbol{B}_\mu$ is an effective magnetic field generated by externally applied microwave radiation. Unlike in the conventional Ising model [9], spin–spin coupling is not restricted to nearest neighbours on the lattice, but extends over all pairs of ions. The coupling coefficients $J_{i,j}$ can be expressed in terms of the transverse phonon eigenfunctions of the lattice and a few other experimental parameters (Eq. (4) of [10]). A numerical evaluation of that expression for the given lattice geometry shows that the approximation $J_{i,j} \propto D_{i,j}^{-\alpha}$ holds to a very good degree [6]. Here $D_{i,j}$ denotes the Euclidean distance between sites i and j on the lattice, and α is an exponent that can in principle be tuned within the range $0 \leq \alpha \leq 3$ by varying the difference in frequency of two off-resonant lasers used in the experiment. The absolute values and even the signs of the coefficients $J_{i,j}$ can also be tuned, allowing for the investigation of ferromagnetic as well as anti-ferromagnetic couplings. In the latter case, due to geometric frustration on the triangular lattice, spin liquids and other exotic quantum phases may possibly occur. It should be feasible to efficiently simulate the behavior of a long-range quantum Ising model on a triangular lattice with several hundred trapped ions, well beyond system sizes that can be dealt with in numerical simulations. However, this will be true only if the assumptions used in [8] for the derivation of (1) are indeed satisfied in the experiment. To date, the Penning ion trap simulator has been benchmarked only

through comparison with mean field theory, a classical limit of (1) where quantum fluctuations and correlations are ignored. The exact results of this Letter enable a much higher level of benchmarking, and a determination of the time scales over which the expected emulation of quantum effects of an Ising model is indeed realized. The results can also be applied to the linear radio-frequency ion trap quantum simulators [11] and, along similar lines, benchmarking of quantum magnets emulated by means of ultracold molecules should be possible [12].

For the theoretical analysis of relaxation times and the decay of correlations, we study a model which is more general than the Hamiltonian in (1) in some respects, and more restricted in others: We generalize to lattices of arbitrary spatial dimension d and arbitrary lattice structure, but come back to the two-dimensional triangular lattice later in this Letter. The effective magnetic field $\boldsymbol{B}_\mu$ in (1) is required to point in z direction, yielding a Hamiltonian of the form

$$H_\ell = -\sum_{i<j} J_{i,j}\sigma_i^z\sigma_j^z - B\sum_i \sigma_i^z, \tag{2}$$

where the index ℓ indicates the presence of a longitudinal field B. At first sight it may look as if the resulting problem is purely classical, as all terms in H_ℓ commute with each other, and equilibrium properties such as the partition function are indeed identical to those of the corresponding classical Ising model. For nonequilibrium calculations, however, quantumness enters through observables and/or initial density operators that do not commute with the Hamiltonian (2), and entanglement and other genuine quantum properties may be present. Observables consisting only of σ_i^z operators commute with the Hamiltonian and therefore show no relaxation behavior, but other observables do, as we will confirm in the following. In spite of its simplicity, the model (2) exhibits non-trivial and remarkably rich nonequilibrium behavior.

To study the relaxation to equilibrium in this model, we want to compute the time evolution of spin–spin correlations

$$\left\langle \sigma_i^x\sigma_j^x \right\rangle(t) = \mathrm{Tr}\left(\mathrm{e}^{\mathrm{i}H_\ell t}\sigma_i^x\sigma_j^x\mathrm{e}^{-\mathrm{i}H_\ell t}\rho_0\right) \tag{3}$$

in units of $\hbar = 1$. A significant simplification is achieved by restricting the initial states to density operators ρ_0 that are diagonal matrices in the σ^x tensor-product eigenbasis. This idea has been used in [13, 14] for the computation of expectation values of a rather restricted class of 1-spin observables. In the present Letter, these restrictions are relaxed and the exact analytic calculations are extended to correlation functions for arbitrary finite system sizes. Details of the calculation are reported in the Supplementary Material. For vanishing longitudinal magnetic field $B = 0$, the final results are

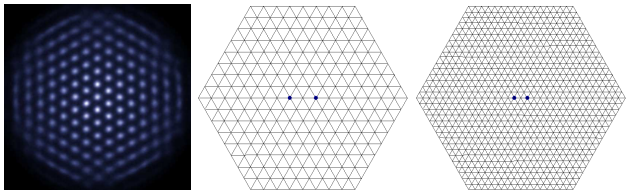

FIG. 1. (Color online) Left: A top-view resonance fluorescence image showing the center region of an ion crystal captured in the ions' rest frame. Fluorescence is an indication of a valence electron being in the spin-up state. Here, all ions are in the spin-up state. The lattice constant is approximately 20 μm. Center and right: Triangular lattices on hexagonal patches of side lengths $L = 8$ and 16.

$$\left\langle \sigma_i^x\sigma_j^y \right\rangle(t) = \left\langle \sigma_i^x\sigma_j^z \right\rangle(t) = \left\langle \sigma_i^z\sigma_j^z \right\rangle(t) = 0, \tag{4a}$$

$$\left\langle \sigma_i^y\sigma_j^z \right\rangle(t) = \langle \sigma_i^x\rangle(0)\sin\left(2tJ_{i,j}\right)\prod_{k\neq i,j}\cos\left(2tJ_{i,k}\right), \tag{4b}$$

$$\left\langle \sigma_i^x\sigma_j^x \right\rangle(t) = P_{i,j}^- + P_{i,j}^+, \quad \left\langle \sigma_i^y\sigma_j^y \right\rangle(t) = P_{i,j}^- - P_{i,j}^+, \tag{4c}$$

with

$$P_{i,j}^\pm = \frac{1}{2}\left\langle \sigma_i^x\sigma_j^x \right\rangle(0)\prod_{k\neq i,j}\cos\left[2\left(J_{k,i}\pm J_{k,j}\right)t\right]. \tag{4d}$$

These expressions are valid for arbitrary coupling constants $J_{i,j}$, and therefore apply in arbitrary spatial dimension and on arbitrary lattices. Moreover they can easily be evaluated on a personal computer for millions of spins. The presence of a longitudinal magnetic field $B \neq 0$ modifies Eqs. (4a)–(4d) by imposing an additional spin precession at an angular frequency proportional to B (Supplementary Material). For the relaxation to equilibrium we are interested in, precession turns out to be irrelevant and we will discuss the $B = 0$ case in the following. A generalization to arbitrary n-spin correlation functions is also straightforward. Since any operator on $\mathbb{C}^{2^N}$ can be expanded in terms of products of Pauli operators, such results for correlation functions of arbitrary order permit in principle the computation of the time-evolution of arbitrary operators. This does not add much to the discussion of the physical phenomena we are interested in here, and we will therefore restrict the discussion to 2-spin correlations.

As an example, the time evolution of spin–spin correlations is illustrated for system parameters similar to those of the ion trap experiments of Britton *et al.* [6]: We consider hexagonal patches of triangular lattices (Fig. 1), and $J_{i,j} = JD_{i,j}^{-\alpha}$ proportional to the αth power of the inverse Euclidean distance of sites i and j on that lattice, with J being a coupling constant. The plots in Fig. 2 suggest that correlations decay to their microcanonical equilibrium values $\langle\sigma_i^a\sigma_j^b\rangle_{\mathrm{mc}} = 0$ where $a, b \in \{x, y, z\}$, but this decay is only apparent: Since the expressions in

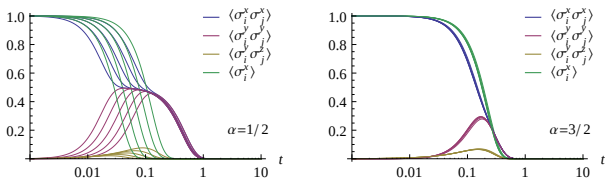

FIG. 2. (Color online) Time evolution of the (normalized) spin–spin correlations as given by (4a)–(4d). The lattice sites i and j are chosen one lattice site to the right, respectively left, of the center of the hexagonal patch, as indicated by the blue dots in Fig. 1 (center and right). The various curves of the same color in each plot correspond to side lengths $L = 4$, 8, 16, 32, and 64 (from right to left) of the hexagonal patches. The left panel is for power law interactions with exponent $\alpha = 1/2$, but results are qualitatively similar for all α between zero and $d/2$. The right panel is for $\alpha = 3/2$, with qualitatively similar results for all $\alpha > d/2$. The unit of time is $1/J$.

(4b)–(4d) consist of products of N trigonometric functions, the evolution in time of spin–spin correlations is quasi-periodic for any finite number N of spins, and relaxation to equilibrium cannot occur in the strong sense. Instead, recurrences will repeatedly bring the system arbitrarily close to its initial state. These recurrences occur on a time scale that is exponentially large in N and, already for moderate system sizes, do not show up on the time scales plotted in Fig. 2. (For example, for a lattice with side length $L = 4$ and $\alpha = 3/2$, the first significant recurrence occurs at a time three orders of magnitude larger than the relaxation time). For a mathematical analysis, however, the recurrences may pose an obstacle. In order to study relaxation to equilibrium in a meaningful way, one can either resort to a weaker (probabilistic) notion of equilibrium [5], or, and this is the strategy we use, suppress the quasi-periodic recurrences by working in the thermodynamic limit $N \to \infty$. With (4b)–(4d) as a starting point, we have derived upper bounds on the time evolution of spin–spin correlations in the thermodynamic limit for a few different lattice structures, and it turns out that they are all of the form

$$\langle\sigma_i^x\sigma_j^x\rangle(t),\ \langle\sigma_i^y\sigma_j^y\rangle(t) \leq \bar{P}_{i,j}^- + \bar{P}_{i,j}^+ \tag{5a}$$

with

$$\bar{P}_{i,j}^\pm \leq \frac{1}{2}\langle\sigma_i^x\sigma_j^x\rangle(0)\exp\left[-C_{i,j}^\pm(\alpha)N^{q^\pm(\alpha)}t^{p^\pm(\alpha)}\right], \tag{5b}$$

with $q^+(\alpha) = \max\{0, 1-2\alpha/d\}$, $q^-(\alpha) = 0$, $p^+(\alpha) = \min\{2, d/\alpha\}$, and $p^-(\alpha) = d/(1+\alpha)$. The constants C depend on the exponent α and the lattice structure. Other 2-spin correlation functions have similar properties, and details of the derivation are provided in the Supplementary Material. For the example of a triangular lattice in two dimensions with $\alpha = 3/2$ and i, j as in Fig. 1, we obtain $C_{i,j}^+ \approx 11.04$ and $C_{i,j}^- \approx 1.119$, and the corresponding bound (5a) is compared to exact finite-system results in Fig. 3 (left). In contrast with the exponential decay of correlations in the nearest-neighbor Ising model [15], the bound (5b) reveals a compressed exponential decay for $\alpha < d/2$, and a stretched exponential decay otherwise—even for large α, where power-law couplings are expected to correspond to nearest-neighbor interactions in the limit $\alpha \to \infty$.

There are other, and even more striking, α dependent aspects of the relaxation dynamics: The plot in the right panel of Fig. 2, representative for exponents $\alpha \geq 1$, shows a simple relaxation to equilibrium with a single relevant time scale. The left panel of Fig. 2, representative for exponents $0 \leq \alpha \leq 1$, differs considerably: In a first step, the $\sigma_i^x\sigma_j^x$ and $\sigma_i^y\sigma_j^y$ correlations display a Gaussian decay on a fast timescale τ_1 to precisely 1/2 of the $\sigma_i^x\sigma_j^x$ initial value, before finally relaxing to their vanishing equilibrium value on a much longer timescale τ_2. τ_1 coincides with the timescale on which 1-spin observables (green lines in Fig. 2) relax, while correlations are not yet equilibrated. Then the system remains *prethermalized* [16] for a relatively long period of time, a behavior observed in the left panel of Fig. 2 as a conspicuous plateau. Different from earlier observations of prethermalization in quantum dynamics, the ratio τ_1/τ_2 goes to zero in the large-N limit, i.e., separation of timescales become more pronounced with increasing system size. We believe that such a behavior is peculiar to long-range interacting systems, as it bears some similarity to divergent (with N) relaxation timescales as observed for classical long-range systems in the astrophysical context [17]. Similarly, the separation of timescales becomes more pronounced also in the limit $\alpha \to 0$, in which the slow relaxation timescale diverges. This fact may be explained by the presence of $N(N-1)$ additional symmetries in the $\alpha = 0$ case, where all operators $\sigma_i^x\sigma_j^x + \sigma_i^y\sigma_j^y$ commute with the Hamiltonian (2). Although these symmetries are absent for $\alpha \gtrsim 0$, the slow timescale can be seen as a remnant of the weakly destroyed $\alpha = 0$ symmetry. While 2-spin correlations may exhibit relaxation in a two-step process, we have checked that no third timescale emerges when the calculations are generalized to 3-spin correlations.

Multiple timescales of relaxation may emerge for various reasons. One possible scenario that has been observed previously, both in theory and experiment [18], is that dephasing is responsible for prethermalization, while a collisional mechanism causes relaxation on a slower timescale. In order to test which of these mechanism is at work in the long-range Ising model, we have computed the time evolution of the n-spin purity

$$\gamma_n(t) = \mathrm{Tr}\left(\rho_n^2(t)\right), \tag{6}$$

where ρ_n is the n-spin reduced density operator, as obtained by tracing the density operator ρ over all but n spins. Knowledge of the 1-spin expectation values $\langle\sigma_i^x\rangle$, $\langle\sigma_i^y\rangle$, and $\langle\sigma_i^z\rangle$ allows for the reconstruction of ρ_1, and

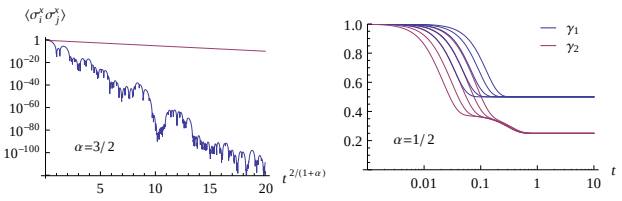

FIG. 3. (Color online) Left: Upper bound (5a) (straight red line) compared to the exact time evolution (4c) (wiggly blue line) of the spin–spin correlator $\langle\sigma_i^x\sigma_j^x\rangle(t)/\langle\sigma_i^x\sigma_j^x\rangle(0)$, plotted *vs.* rescaled time $t^{2/(1+\alpha)}$. The linearly decaying trend in the plot, superimposed by fluctuations, confirms the asymptotic behavior over a range of more than hundred orders of magnitude. Right: Time evolution of the 1- and 2-spin purities γ_1 and γ_2 as defined in (6). Each relaxation step in spin–spin correlations in Fig. 2 is accompanied by a drop in γ_2. This suggests that dephasing is responsible for all relaxation steps.

additional knowledge of the spin–spin correlations (4a)–(4d) facilitates reconstruction of ρ_2. For the long-range Ising model, as shown in Fig. 3 (right) for $\alpha = 1/2$, both relaxation steps of spin–spin correlations turn out to be associated with a drop in the purity γ_2, and this is an indication that both relaxation steps are caused by dephasing. In contrast, a collisional relaxation would be characterized by a redistribution of mode occupation numbers or probabilities and requires inelastic scattering processes between these modes. Since the Ising model (2) has only commuting terms, no inelastic collisional mechanism is available.

In the trapped ion simulator of [6], spontaneous emission from the off-resonant laser beams used to engineer the long-range Ising interaction (1) sets one experimental time scale that, over longer intervals of time, the system can no longer be considered isolated. However, we calculate that with upgrades to the set-up described in [6], the quantum many-body relaxation time scales can be short compared to the spontaneous emission time scale. Specifically, with $N = 217$ ions and an optical dipole force generated from two 10 mW beams crossing with an angular separation of 35^o (see Fig. 1 of [6]) and frequency difference tuned to generate an $\alpha = 1/2$ power law interaction, we calculate the two relaxation timescales corresponding to $P_{i,j}^{\pm}$ in (4d) to be ≈ 30 μs and ≈ 430 μs, respectively. The spontaneous emission time for this configuration is $(1/\Gamma) \sim 4$ ms. All of these time scales are short compared to the $T_2 \gtrsim 50$ ms coherence time of the Be^+ valence electron spin qubits.

To compare with the exact results reported here requires an experimental measurement of the spin-spin correlations after the Ising interaction has been applied for a variable period. This is readily accomplished with trapped ions. Reference [6] uses state-dependent resonance fluorescence to measure spin orientation in the σ^z basis. Specifically global fluorescence collected from all the ions in the array is used to measure the global spin state of the system (i.e., the total number of spins in the $|\uparrow\rangle_z$ state and the total number of spins in the $|\downarrow\rangle_z$ state). Shot-to-shot fluctuations in these measurements are sensitive to the second-order moment $\langle J_z^2\rangle$ of the total z-component of the spin $J_z \equiv \sum_{i=1}^N \sigma_i^z/2$. Of particular interest are measurements of the second-order moments in directions perpendicular to the mean composite spin vector. For example, with all spins initially pointing along the x-axis, fluctuations in measurements of J_z after rotation about the x-axis by an angle θ are sensitive to

$$\langle J_z^2\rangle_\theta = \sum_{i,j=1}^{N} \frac{1}{4}\big[\sin^2\theta\,\langle\sigma_i^y\sigma_j^y\rangle - \sin\theta\cos\theta\,\langle\sigma_i^y\sigma_j^z + \sigma_i^z\sigma_j^y\rangle + \cos^2\theta\,\langle\sigma_i^z\sigma_j^z\rangle\big]. \quad (7)$$

These spin-squeezing measurements [19] are sensitive to pairwise correlations summed over all the spins in the ensemble. In addition to global fluorescence measurements, the top-view image in Fig. 1 (left) indicates that individual spin detection may also be possible in this system. Individual spin detection is complicated by the rotational stability of the crystal, but has significant advantages in the reduction of potential sources of noise in the second-order moment measurements, as well as permitting a microscopic measurement of the spin state of the system.

Once such a quantum simulator is benchmarked, it may in turn be used for the testing of more general approximate theories. Moreover, there are certain phenomena which are believed to be peculiar to long-range interacting systems and which might receive their first experimental confirmation in the ion trap set-up. One example is the threshold at $\alpha = d/2$ below which a second timescale of relaxation emerges. There is evidence that not only the existence of this dynamical long-range threshold, but also its numerical value $d/2$, is universal for classical as well as quantum mechanical long-range interacting systems [20]. Other long-range peculiarities include nonequivalent equilibrium statistical ensembles, a phenomenon that has been known in the astrophysical context for decades [21] but has not seen experimental verification in a tabletop experiment.

In summary, under convenient restrictions on the initial conditions, we have obtained exact analytic results for spin–spin correlations of long-range quantum Ising models in arbitrary spatial dimensions and for various lattice structures. Prethermalization, widely separated timescales, and other phenomena that further our understanding of the timescales governing the relaxation to equilibrium were discussed. Comparison of our analytic results to experimental measurements of spin-spin correlations will enable benchmarking of the trapped-ion quantum simulator of [6] in a regime where quantum effects are paramount. Subsequently, the benchmarked

quantum simulator may be employed to investigate relaxation timescales in parameter regimes and for initial states where analytic results presently are not available.

M. K. acknowledges support by the Incentive Funding for Rated Researchers programme of the National Research Foundation of South Africa. B. C. S. and J. J. B. acknowledge support from the DARPA OLE program. Manuscripts with contributions from the US National Institute of Standards and Technology are not subject to US copyright.

* kastner@sun.ac.za

[1] T. Kinoshita, T. Wenger, and D. S. Weiss, Nature **440**, 900 (2006); S. Hofferberth, I. Lesanovsky, B. Fischer, T. Schumm, and J. Schmiedmayer, Nature **449**, 324 (2007); S. Trotzky, Y.-A. Chen, A. Flesch, I. P. McCulloch, U. Schollwöck, J. Eisert, and I. Bloch, Nature Phys. **8**, 325 (2012).
[2] M. A. Cazalilla and M. Rigol, New J. Phys. **12**, 055006 (2010).
[3] A. Polkovnikov, K. Sengupta, A. Silva, and M. Vengalattore, Rev. Mod. Phys. **83**, 863 (2011).
[4] J. M. Deutsch, Phys. Rev. A **43**, 2046 (1991); M. Srednicki, Phys. Rev. E **50**, 888 (1994); M. Rigol, V. Dunjko, and M. Olshanii, Nature **452**, 854 (2008).
[5] P. Reimann, Phys. Rev. Lett. **101**, 190403 (2008); N. Linden, S. Popescu, A. J. Short, and A. Winter, Phys. Rev. E **79**, 061103 (2009); S. Goldstein, J. L. Lebowitz, C. Mastrodonato, R. Tumulka, and N. Zanghì, Phys. Rev. E **81**, 011109 (2010); A. J. Short and T. C. Farrelly, New J. Phys. **14**, 013063 (2012); P. Reimann and M. Kastner, New J. Phys. **14**, 043020 (2012).
[6] J. W. Britton, B. C. Sawyer, A. C. Keith, C.-C. J. Wang, J. K. Freericks, H. Uys, M. J. Biercuk, and J. J. Bollinger, Nature **484**, 489 (2012).
[7] F. Mintert and C. Wunderlich, Phys. Rev. Lett. **87**, 257904 (2001).
[8] D. Porras and J. I. Cirac, Phys. Rev. Lett. **92**, 207901 (2004).
[9] E. Ising, Z. Phys. **31**, 253 (1925).
[10] K. Kim, M.-S. Chang, R. Islam, S. Korenblit, L.-M. Duan, and C. Monroe, Phys. Rev. Lett. **103**, 120502 (2009).
[11] A. Friedenauer, H. Schmitz, J. T. Glueckert, D. Porras, and T. Schaetz, Nature Phys. **4**, 757 (2008); R. Islam, E. E. Edwards, K. Kim, S. Korenblit, C. Noh, H. Carmichael, G.-D. Lin, L.-M. Duan, C.-C. J. Wang, J. Freericks, and C. Monroe, Nat. Commun. **2**, 377 (2011); B. P. Lanyon, C. Hempel, D. Nigg, M. Müller, R. Gerritsma, F. Zähringer, P. Schindler, J. T. Barreiro, M. Rambach, G. Kirchmair, M. Hennrich, P. Zoller, R. Blatt, and C. F. Roos, Science **334**, 57 (2011).
[12] K. R. A. Hazzard, S. R. Manmana, M. Foss-Feig, and A. M. Rey, "Far from equilibrium quantum magnetism with ultracold atoms," arXiv:1209.4076.
[13] G. G. Emch, J. Math. Phys. **7**, 1198 (1966).
[14] M. Kastner, Phys. Rev. Lett **106**, 130601 (2011); Cent. Eur. J. Phys. **10**, 637 (2012).
[15] P. Calabrese, F. H. L. Essler, and M. Fagotti, Phys. Rev. Lett. **106**, 227203 (2011).
[16] M. Moeckel and S. Kehrein, Phys. Rev. Lett. **100**, 175702 (2008).
[17] A. Gabrielli, M. Joyce, and B. Marcos, Phys. Rev. Lett. **105**, 210602 (2010).
[18] M. Gring, M. Kuhnert, T. Langen, T. Kitagawa, B. Rauer, M. Schreitl, I. Mazets, D. A. Smith, E. Demler, and J. Schmiedmayer, Science **337**, 1318 (2012).
[19] H. Uys, M. J. Biercuk, J. Britton, and J. J. Bollinger, "Towards spin squeezing with trapped ions," arXiv:1111.4792.
[20] R. Bachelard and M. Kastner, "A dynamical long-range threshold," In preparation.
[21] W. Thirring, Z. Phys. **235**, 339 (1970).

Supplementary Material

Appendix A: Exact calculation of spin–spin correlations for finite N

Starting point of the calculation is the general expression of the expectation value

$$\left\langle \sigma_i^{\pm}\sigma_j^{\pm}\right\rangle(t) = \mathrm{Tr}\left(\mathrm{e}^{\mathrm{i}H_\ell t}\sigma_i^{\pm}\sigma_j^{\pm}\mathrm{e}^{-\mathrm{i}H_\ell t}\rho_0\right) \tag{A.1}$$

with respect to the initial density operator ρ_0, where we assume ρ_0 to be diagonal in the σ_x tensor product eigenbasis. Spin ladder operators are defined as $\sigma^{\pm} = (\sigma^x \pm \mathrm{i}\sigma^y)/2$. Since all terms in the Hamiltonian H_ℓ commute, we can factorize the time evolution operator,

$$\exp\left(-\mathrm{i}H_\ell t\right) = \prod_{k<l}\exp\left(\mathrm{i}J_{k,l}\sigma_k^z\sigma_l^z t\right)\prod_m \exp\left(\mathrm{i}B\sigma_m^z t\right), \tag{A.2}$$

and similarly for the Hermitian conjugate. All factors in (A.2) that contain neither σ_i^z nor σ_j^z commute with $\sigma_i^{\pm}\sigma_j^{\pm}$. To compute the time evolution in (A.1), we therefore have to deal with the expression

$$\begin{aligned}\prod_{k\neq i,j}\exp\left(-\mathrm{i}J_{k,i}\sigma_k^z\sigma_i^z t\right)\exp\left(-\mathrm{i}J_{k,j}\sigma_k^z\sigma_j^z t\right)\exp\left(-\mathrm{i}B\sigma_i^z t\right)\\ \times\exp\left(-\mathrm{i}B\sigma_j^z t\right)\sigma_i^{\pm}\sigma_j^{\pm}\exp\left(\mathrm{i}B\sigma_j^z t\right)\exp\left(\mathrm{i}B\sigma_i^z t\right)\\ \times\prod_{l\neq i,j}\exp\left(\mathrm{i}J_{l,j}\sigma_l^z\sigma_j^z t\right)\exp\left(\mathrm{i}J_{l,i}\sigma_l^z\sigma_i^z t\right).\end{aligned} \tag{A.3}$$

Making use of $[\sigma^z,\sigma^{\pm}] = \pm 2\sigma^{\pm}$, the time evolution due to the magnetic field B simplifies to

$$\begin{aligned}\exp\left(-\mathrm{i}B\sigma_i^z t\right)\exp\left(-\mathrm{i}B\sigma_j^z t\right)\sigma_i^{\pm}\sigma_j^{\pm}\exp\left(\mathrm{i}B\sigma_j^z t\right)\\ \times\exp\left(\mathrm{i}B\sigma_i^z t\right) = \sigma_i^{\pm}\sigma_j^{\pm}\exp\left(\mp 4\mathrm{i}Bt\right).\end{aligned} \tag{A.4}$$

Picking one lattice site $k \neq i,j$, the time evolution of $\sigma_i^{\pm}\sigma_j^{\pm}$ due to the interaction with the spin at k can be written as

$$\begin{aligned}\exp\left(-\mathrm{i}J_{k,i}\sigma_k^z\sigma_i^z t\right)\exp\left(-\mathrm{i}J_{k,j}\sigma_k^z\sigma_j^z t\right)\sigma_i^{\pm}\sigma_j^{\pm}\\ \times\exp\left(\mathrm{i}J_{k,j}\sigma_k^z\sigma_j^z t\right)\exp\left(\mathrm{i}J_{k,i}\sigma_k^z\sigma_i^z t\right)\\ = \sigma_i^{\pm}\sigma_j^{\pm}\cos\left[2t(J_{i,k}+J_{j,k})\right]\\ \mp\mathrm{i}\sigma_i^{\pm}\sigma_j^{\pm}\sigma_k^z\sin\left[2t(J_{i,k}+J_{j,k})\right].\end{aligned} \tag{A.5}$$

Since the initial state ρ_0 is assumed to be diagonal in the σ_x tensor product eigenbasis, only diagonal elements of the operator $\mathrm{e}^{\mathrm{i}H_\ell t}\sigma_i^{\pm}\sigma_j^{\pm}\mathrm{e}^{-\mathrm{i}H_\ell t}$ in the same basis contribute to the trace in (A.1). For this reason we can drop the second term on the right-hand side of (A.5), as it is proportional to σ_k^z. Inserting (A.4) and (A.5) into (A.1), we obtain

$$\begin{aligned}\left\langle \sigma_i^{\pm}\sigma_j^{\pm}\right\rangle(t) = \left\langle \sigma_i^{\pm}\sigma_j^{\pm}\right\rangle(0)\exp\left(\mp 4\mathrm{i}Bt\right)\\ \times\prod_{k\neq i,j}\cos\left[2t(J_{i,k}+J_{j,k})\right],\end{aligned} \tag{A.6a}$$

where $\left\langle \sigma_i^{\pm}\sigma_j^{\pm}\right\rangle(0) = \mathrm{Tr}\left(\sigma_i^{\pm}\sigma_j^{\pm}\rho_0\right)$. A similar calculation yields

$$\left\langle \sigma_i^{\pm}\sigma_j^{\mp}\right\rangle(t) = \left\langle \sigma_i^{\pm}\sigma_j^{\mp}\right\rangle(0)\prod_{k\neq i,j}\cos\left[2t(J_{i,k}-J_{j,k})\right], \tag{A.6b}$$

a notable difference to (A.6a) being that the presence of an external magnetic field B has no effect on this expectation value. From

$$4\sigma_i^{\pm}\sigma_j^{\pm} = \sigma_i^x\sigma_j^x - \sigma_i^y\sigma_j^y \pm \mathrm{i}\sigma_i^x\sigma_j^y \pm \mathrm{i}\sigma_i^y\sigma_j^x, \tag{A.7a}$$

$$4\sigma_i^{\pm}\sigma_j^{\mp} = \sigma_i^x\sigma_j^x + \sigma_i^y\sigma_j^y \mp \mathrm{i}\sigma_i^x\sigma_j^y \pm \mathrm{i}\sigma_i^y\sigma_j^x, \tag{A.7b}$$

we obtain

$$\sigma_i^x\sigma_j^x = \quad 2\Re\left(\sigma_i^{\pm}\sigma_j^{\mp} + \sigma_i^{\pm}\sigma_j^{\pm}\right), \tag{A.8a}$$

$$\sigma_i^y\sigma_j^y = \quad 2\Re\left(\sigma_i^{\pm}\sigma_j^{\mp} - \sigma_i^{\pm}\sigma_j^{\pm}\right), \tag{A.8b}$$

$$\sigma_i^x\sigma_j^y = \mp 2\Im\left(\sigma_i^{\pm}\sigma_j^{\mp} - \sigma_i^{\pm}\sigma_j^{\pm}\right), \tag{A.8c}$$

$$\sigma_i^y\sigma_j^x = \pm 2\Im\left(\sigma_i^{\pm}\sigma_j^{\mp} + \sigma_i^{\pm}\sigma_j^{\pm}\right), \tag{A.8d}$$

and furthermore, using the properties of the initial density operator ρ_0,

$$4\left\langle \sigma_i^{\pm}\sigma_j^{\pm}\right\rangle(0) = 4\left\langle \sigma_i^{\pm}\sigma_j^{\mp}\right\rangle(0) = \left\langle \sigma_i^x\sigma_j^x\right\rangle(0). \tag{A.9}$$

Inserting (A.6a), (A.6b) and (A.9) into (A.8a)–(A.8d), we arrive at the final expressions

$$\left\langle \sigma_i^x\sigma_j^x\right\rangle(t) = P_{i,j}^- + \cos(4Bt)P_{i,j}^+, \tag{A.10a}$$

$$\left\langle \sigma_i^y\sigma_j^y\right\rangle(t) = P_{i,j}^- - \cos(4Bt)P_{i,j}^+, \tag{A.10b}$$

$$\left\langle \sigma_i^x\sigma_j^y\right\rangle(t) = -\sin(4Bt)P_{i,j}^+, \tag{A.10c}$$

with $P_{i,j}^{\pm}$ as defined in (5d). A similar calculate yields

$$\left\langle \sigma_i^x\sigma_j^z\right\rangle(t) = \sin(2Bt)P_{i,j}^z, \quad \left\langle \sigma_i^y\sigma_j^z\right\rangle(t) = \cos(2Bt)P_{i,j}^z, \tag{A.10d}$$

with

$$P_{i,j}^z = -\left\langle \sigma_i^x\right\rangle(0)\sin(2tJ_{i,j})\prod_{k\neq i,j}\cos(2tJ_{i,k}). \tag{A.10e}$$

Finally, from symmetry considerations we obtain

$$\left\langle \sigma_i^z\sigma_j^z\right\rangle(t) = 0. \tag{A.10f}$$

A generalization of these calculations to n-spin correlation functions is straightforward, yielding for example

$$\begin{aligned}\left\langle \sigma_i^{\pm}\sigma_j^{\pm}\sigma_k^{\pm}\right\rangle(t) = \left\langle \sigma_i^{\pm}\sigma_j^{\pm}\sigma_k^{\pm}\right\rangle(0)\exp\left(\mp 6\mathrm{i}Bt\right)\\ \times\prod_{l\neq i,j,k}\cos\left[2t(J_{i,l}+J_{j,l}+J_{k,l})\right],\end{aligned} \tag{A.11}$$

and similar expressions for other correlation functions.

Appendix B: Upper bounds on spin–spin correlations in the thermodynamic limit

In the thermodynamic limit of infinite system size, a bound on the product

$$\mathcal{P}_{i,j}^{\pm} = \prod_{\substack{k=1 \\ k\neq i,j}}^{N} \left|\cos\left[2\left(J_{k,i} \pm J_{k,j}\right)t\right]\right| \tag{B.12}$$

in Eq. (5d) with $J_{i,j} = D_{i,j}^{-\alpha}$ and $\alpha \geq 0$ is derived. For any given t, one can find a compact region $g_{i,j}^{\pm}(t)$ (containing i and j) of the infinite triangular lattice G such that

$$|2(J_{k,i} \pm J_{k,j})t| < \pi/2 \tag{B.13}$$

for all $k \in G \setminus g_{i,j}^{\pm}(t)$. Since $|\cos x| \leq 1$, we have

$$\mathcal{P}_{i,j}^{\pm} \leq \prod_{k\notin g_{i,j}^{\pm}(t)} \left|\cos\left[2\left(J_{k,i} \pm J_{k,j}\right)t\right]\right|. \tag{B.14}$$

Next, using the inequality

$$|\cos x| \leq 1 - \left(\frac{2x}{\pi}\right)^2 \leq \exp\left[-\left(\frac{2x}{\pi}\right)^2\right] \qquad \text{for } x < \pi/2, \tag{B.15}$$

we obtain

$$\mathcal{P}_{i,j}^{\pm} \leq \exp\left[-\frac{16t^2}{\pi^2} \sum_{k\notin g_{i,j}^{\pm}(t)} \left(J_{k,i} \pm J_{k,j}\right)^2\right]. \tag{B.16}$$

For simplicity, we consider lattice sites i and j symmetrically arranged to the right and left of lattice site 0, as illustrated below for the example of distance $\delta = D_{i,j} = 2$, but other arrangements can be treated in a similar way.

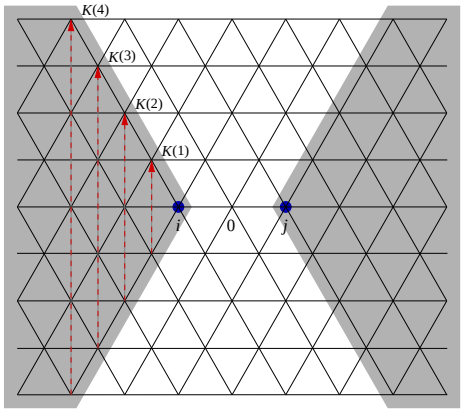

Disregarding all sites that lie outside the grey shaded area $h_{i,j}$ in the above illustration, we obtain a lower bound on the sum in (B.16),

$$\sum_{k\in G\setminus g_{i,j}^{\pm}(t)} \left(J_{k,i} \pm J_{k,j}\right)^2 \geq \sum_{k\in h_{i,j}\cap(G\setminus g_{i,j}^{\pm}(t))} \left(J_{k,i} \pm J_{k,j}\right)^2. \tag{B.17}$$

Each individual summand $\left(J_{k,i} \pm J_{k,j}\right)^2$ can be minorized by $\left(J_{K,i} \pm J_{K,j}\right)^2$, where K is determined from k by going vertically upwards along the dashed (red) line in the above illustration until a boundary point of the shaded region is reached. To a boundary point labeled by $K(r)$ there correspond $r+1$ points in the sum, and this allows us to bound the sum by

$$\sum_{k\in G\setminus g_{i,j}^{\pm}(t)} \left(J_{k,i} \pm J_{k,j}\right)^2 \geq 2J^2 \sum_{r=R_0^{\pm}(t)}^{R} r\left(D_{i,K(r)}^{-\alpha} \pm D_{j,K(r)}^{-\alpha}\right)^2. \tag{B.18}$$

To exclude lattice sites in the region $g_{i,j}^{\pm}(t)$, i.e., in order to satisfy the inequality (B.13) used earlier, $R_0^{\pm}(t)$ has to be chosen large enough. An asymptotic analysis of (B.13) shows that this condition can be implemented by choosing

$$R_0^{+}(t) > \left(\frac{8Jt}{\pi}\right)^{1/\alpha}, \qquad R_0^{-}(t) \sim \left(\frac{4\alpha Jt}{\pi}\right)^{1/(1+\alpha)}, \tag{B.19}$$

where the condition on $R_0^{+}(t)$ works always, the one for $R_0^{-}(t)$ only for sufficiently large t. Inserting the distances

$$D_{i,K(r)} = r, \qquad D_{j,K(r)} = \sqrt{\delta^2 + r\delta + r^2} \tag{B.20}$$

and bounding the sum by an integral, we obtain

$$\mathcal{P}_{i,j}^{\pm} \leq \exp\left[-\frac{32J^2t^2}{\pi^2} \int_{R_0^{\pm}(t)}^{R} \mathrm{d}r\, r\left(\frac{1}{r^\alpha} \pm \frac{1}{\sqrt{\delta^2 + r\delta + r^2}^{\alpha}}\right)^2\right], \tag{B.21}$$

valid in the limit of large R. Since we are interested in the limit of large R and t, we can expand the integrand to leading order in $1/r$, obtaining

$$r\left(\frac{1}{r^\alpha} + \frac{1}{\sqrt{\delta^2 + r\delta + r^2}^{\alpha}}\right)^2 \sim 4r^{1-2\alpha}, \tag{B.22a}$$

$$r\left(\frac{1}{r^\alpha} - \frac{1}{\sqrt{\delta^2 + r\delta + r^2}^{\alpha}}\right)^2 \sim \left(\frac{\alpha\delta}{2}\right)^2 r^{-1-2\alpha}. \tag{B.22b}$$

Inserting these expressions into (B.21), the integral can be solved by elementary means. Making use of the asymptotic equality $R^2 \sim N/3$ and performing the limit $N \to \infty$, we obtain the final results

$$\mathcal{P}_{i,j}^{+} \leq \begin{cases} \exp\left[-\dfrac{64J^2t^2}{\pi^2(1-\alpha)}\left(\dfrac{N}{3}\right)^{1-\alpha}\right] & \text{for } \alpha < 1, \\ \exp\left[-\dfrac{1}{\alpha-1}\left(\dfrac{8Jt}{\pi}\right)^{2/\alpha}\right] & \text{for } \alpha > 1, \end{cases} \tag{B.23a}$$

and

$$\mathcal{P}_{i,j}^{-} \leq \exp\left[-\frac{\delta^2}{4\alpha}\left(\frac{4\alpha Jt}{\pi}\right)^{2/(1+\alpha)}\right], \tag{B.23b}$$

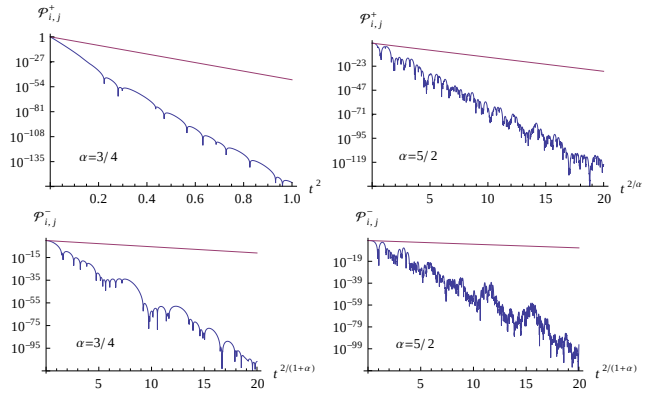

FIG. 4. Logarithmic plot of the products $\mathcal{P}^+_{i,j}$ (top) and $\mathcal{P}^-_{i,j}$ (bottom) as a function of rescaled time $t^{p^\pm(\alpha)}$, evaluated for a hexagonal patch of a triangular lattice with side length $L = 16$ for $\alpha = 3/4$ (left) and $\alpha = 5/2$ (right). The exponents $p^+(\alpha) = \min\{2, 2/\alpha\}$ and $p^-(\alpha) = 2/(1+\alpha)$ of the time rescaling are those predicted by the bounds (B.23a) and (B.23b) for the asymptotic behaviour at large L and t. The linear decaying trend in the plot, superimposed by fluctuations, confirms over a range of more than hundred orders of magnitude that the asymptotic behaviour of $\mathcal{P}^\pm_{i,j}$ is indeed as given by the bounds. The straight lines in the plots are the bounds (B.23a) and (B.23b), indicating that the numerical constants in the exponents of (B.23a) and (B.23b) are, as expected, underestimated.

valid in the limit of large R and t. A comparison of these bounds with an exact evaluation of (B.12) for finite lattices is shown, over more than hundred orders of magnitude, in Fig. 4.